

Closed-Form Approximation of the Total Variation Proximal Operator

Edward P. Chandler, Shirin Shoushtari,
Brendt Wohlberg, and Ulugbek S. Kamilov

Washington University in St. Louis, MO 63130, USA

Los Alamos National Laboratory, Los Alamos, NM 87545, USA

{e.p.chandler, s.shirin, kamilov}@wustl.edu, brendt@lanl.gov

Abstract

Total variation (TV) is a widely used function for regularizing imaging inverse problems that is particularly appropriate for images whose underlying structure is piecewise constant. TV regularized optimization problems are typically solved using proximal methods, but the way in which they are applied is constrained by the absence of a closed-form expression for the proximal operator of the TV function. A closed-form approximation of the TV proximal operator has previously been proposed, but its accuracy was not theoretically explored in detail. We address this gap by making several new theoretical contributions, proving that the approximation leads to a proximal operator of some convex function, that it always decreases the TV function, and that its error can be fully characterized and controlled with its scaling parameter. We experimentally validate our theoretical results on image denoising and sparse-view computed tomography (CT) image reconstruction.

1 Introduction

Inverse problems are typically posed as the estimation of a signal $\mathbf{x} \in \mathbb{R}^n$ from measurements

$$\mathbf{y} = \mathbf{A}\mathbf{x} + \mathbf{e}, \quad (1)$$

where $\mathbf{A} \in \mathbb{R}^{m \times n}$ denotes the *forward operator* and $\mathbf{e} \in \mathbb{R}^m$ represents additive noise. The classical approach to solving such problems is to pose them as an optimization problem

$$\mathbf{x}^* \in \arg \min_{\mathbf{x} \in \mathbb{R}^n} f(\mathbf{x}) \quad \text{with} \quad f(\mathbf{x}) = g(\mathbf{x}) + \lambda h(\mathbf{x}), \quad (2)$$

where g and h represent the data-fidelity and regularization terms, respectively, and $\lambda \geq 0$ is the regularization parameter. When the noise in (1) corresponds to the additive white Gaussian noise (AWGN), it is common to use the squared ℓ_2 data fidelity term $g(\mathbf{x}) = \frac{1}{2} \|\mathbf{y} - \mathbf{A}\mathbf{x}\|_2^2$. One of the most widely used choices for h is total variation (TV) [1], which promotes solutions with a sparse image gradient. While it is no longer competitive for natural imagery, it remains effective for other types of imagery, such as those that occur in scientific or industrial imaging, where the implicit piecewise-constant image model is appropriate.

This research was supported by the Laboratory Directed Research and Development program of Los Alamos National Laboratory under project numbers 20200061DR and 20230771DI.

In this work, we focus on the two most common forms of TV, anisotropic h^a and isotropic h^i , which are defined as

$$h^a(\mathbf{x}) := \sum_{i=1}^n \sum_{j=1}^d |[D_j \mathbf{x}]_i| \quad (3)$$

$$h^i(\mathbf{x}) := \sum_{i=1}^n \sqrt{\sum_{j=1}^d ([D_j \mathbf{x}]_i)^2}, \quad (4)$$

where $\mathbf{D} : \mathbb{R}^n \rightarrow \mathbb{R}^{nd}$ is the discrete gradient operator, n denotes the signal size (e.g. $n = 1024$ in a 32×32 image), and d represents the signal dimension (e.g. $d = 2$ for images).

Gradient descent and related methods are not appropriate for problem (2) when h is the TV function since it is non-smooth, but *proximal methods* [2] are very effective. They are based on the *proximal operator* of a function h , defined as

$$\text{prox}_{\tau h}(z) := \arg \min_{\mathbf{x} \in \mathbb{R}^n} \left\{ \frac{1}{2} \|\mathbf{x} - z\|_2^2 + \tau h(\mathbf{x}) \right\}, \quad (5)$$

where $\tau > 0$ is the proximal scaling parameter. This family of optimization algorithms includes the accelerated proximal gradient method (APGM) [3] and the alternating direction method of multipliers (ADMM) [4].

Unfortunately, there is no closed-form solution to the proximal operator (5) of the TV function, requiring it to be computed using an iterative approach [5] within algorithms such as APGM. These sub-iterations can be avoided via an appropriate ADMM variable splitting strategy [6], but in many cases this just pushes the computational complexity to a different component of the algorithm.

A closed-form approximation to the TV proximal operators was introduced in [7–10], based on the concept of proximal average [11]. While the effectiveness of this approximation was analyzed within the context of APGM, its more general properties as an approximation to the TV proximal operator were not explored in detail, and its application in other proximal algorithms was not considered. In this paper, we address this gap by presenting new theoretical results demonstrating that the operator is indeed a good approximation to the proximal operators of anisotropic and isotropic TV. More specifically, we present two new contributions:

- (1) We provide new theoretical justifications for the approximation in [7–10]. Specifically, we show that it is the proximal operator of some convex function, that it always decreases the TV function, and that its accuracy depends on the scaling parameter of the approximate proximal operator.
- (2) We provide new numerical results that validate our theoretical analysis by using the approximate TV proximal operator within APGM and ADMM algorithms for limited angle computed tomography reconstruction. These numerical results confirm the practical applicability of the approximate proximal operator and are consistent with the theory connecting the approximation accuracy with the scaling parameter.

2 Related Work

The TV regularizer promotes sparse image gradients, producing reconstructed images that are approximately piecewise constant. TV regularization has been demonstrated to be effective in various inverse problems, including image deconvolution, diffraction ultrasound tomography, compressed sensing, and optical tomography [12–29]. APGM [3] is often employed to solve image reconstruction problems with the TV regularizer [5]. However, APGM requires additional sub-iterations to compute the proximal operator of the TV regularizer, which can slow down the overall convergence. While ADMM with an appropriate variable-splitting strategy can be used to avoid these sub-iterations [13], the introduction of an additional auxiliary variable representing the image gradients increases memory requirements.

A fast non-iterative algorithm for solving the 1D TV proximal operator has been proposed [30], but it does not generalize for signals with more than one dimension, such as images. To generalize to an arbitrary number

Algorithm 1 APGM with $\mathcal{S}_\tau(\mathbf{z})$

input: $g, \mathbf{x}_0, \mathbf{z}_0, \mathbf{s}_0 \in \mathbb{R}^n, \gamma > 0, \lambda > 0$, and $\{q_k\}_{k \in \mathbb{N}}$

- 1: **for** $k = 1, 2, \dots$ **do**
- 2: $\mathbf{z}^k = \mathbf{s}^{k-1} - \gamma \nabla g(\mathbf{s}^{k-1})$
- 3: $\mathbf{x}^k = \mathcal{S}_{\gamma\lambda}(\mathbf{z}^k)$
- 4: $\mathbf{s}^k = \mathbf{x}^k + ((q_{k-1} - 1)/q_k)(\mathbf{x}^k - \mathbf{x}^{k-1})$
- 5: **end for**

Algorithm 2 ADMM with $\mathcal{S}_\tau(\mathbf{z})$

input: $g, \mathbf{x}_0, \mathbf{z}_0, \mathbf{s}_0 \in \mathbb{R}^n, \gamma > 0, \lambda > 0$

- 1: **for** $k = 1, 2, \dots$ **do**
- 2: $\mathbf{z}^k = \text{prox}_{\gamma g}(\mathbf{x}^{k-1} - \mathbf{s}^{k-1})$
- 3: $\mathbf{x}^k = \mathcal{S}_{\gamma\lambda}(\mathbf{z}^{k-1} + \mathbf{s}^{k-1})$
- 4: $\mathbf{s}^k = \mathbf{s}^{k-1} + \mathbf{x}^k - \mathbf{z}^k$
- 5: **end for**

of dimensions, a closed-form approximation of the proximal operator for TV was proposed, eliminating the need for sub-iterations [7–10]. The convergence of APGM with this approximation for anisotropic TV was investigated in [9] and for isotropic TV was investigated in [10]. These approximations share a close relationship with image reconstruction techniques using wavelet domain regularization [31]. They can also be viewed as the application of the *proximal average* [11] approximation for the proximal operator of a sum of multiple nonsmooth functions. Cycle spinning is another closely related concept originally introduced for denoising [32], later refined [33], and applied in various imaging inverse problems, including image restoration, MRI reconstruction, 3D CT reconstruction, and computed tomography [34–42].

The convergence of proximal algorithms has been extensively investigated [2]. Our work is more related to the family of *inexact* proximal algorithms that rely on approximations of proximal operators or gradient calculations [43–53]. In particular, our theoretical analysis shows that the approximation in [7–10] leads to an inexact TV proximal operator whose accuracy depends on its scaling parameter, thus enabling its use within existing proximal methods.

3 Approximating Total Variation

3.1 Method

In this section, we present the approximation of the TV proximal operator proposed in [9,10]. The motivation for this approximation is the reduction of the computational complexity of calculating the TV proximal operator from $O(knd)$, where k is the number of sub-iterations, to $O(nd)$. Consider the linear mapping $\mathbf{W} : \mathbb{R}^n \rightarrow \mathbb{R}^{2nd}$ defined as

$$\mathbf{W} := \frac{1}{2\sqrt{d}} \begin{bmatrix} \mathbf{A} \\ \mathbf{D} \end{bmatrix}, \quad \mathbf{A} := [\mathbf{A}_1^\top \cdots \mathbf{A}_d^\top]^\top, \\ \mathbf{D} := [\mathbf{D}_1^\top \cdots \mathbf{D}_d^\top]^\top,$$

where $\mathbf{A}_j : \mathbb{R}^n \rightarrow \mathbb{R}^n$ for $j \in \{1, \dots, d\}$ represents an averaging operator along the j^{th} dimension, and $\mathbf{D}_j : \mathbb{R}^n \rightarrow \mathbb{R}^n$ for $j \in \{1, \dots, d\}$ denotes a discrete gradient operator along the j^{th} dimension. \mathbf{A}_j and \mathbf{D}_j are convolutions along the j^{th} dimension of the signal with the kernels

$$\mathbf{a} = \begin{bmatrix} 1 \\ 1 \end{bmatrix}, \quad \mathbf{d} = \begin{bmatrix} 1 \\ -1 \end{bmatrix},$$

respectively. The mapping \mathbf{W} can be interpreted as a union of scaled and shifted first-level discrete Haar wavelet and scaling functions across all d dimensions [9]. It is important to note that this operator satisfies $\mathbf{W}^\top \mathbf{W} = \mathbf{I}$, but due to redundancy in the union of scaled orthogonal transforms, $\mathbf{W} \mathbf{W}^\top \neq \mathbf{I}$ [54].

The approximate TV proximal operator is defined as

$$\mathcal{S}_\tau(\mathbf{z}) := \mathbf{W}^\top \mathcal{T}_{\tau 2\sqrt{d}}(\mathbf{W} \mathbf{z}), \tag{6}$$

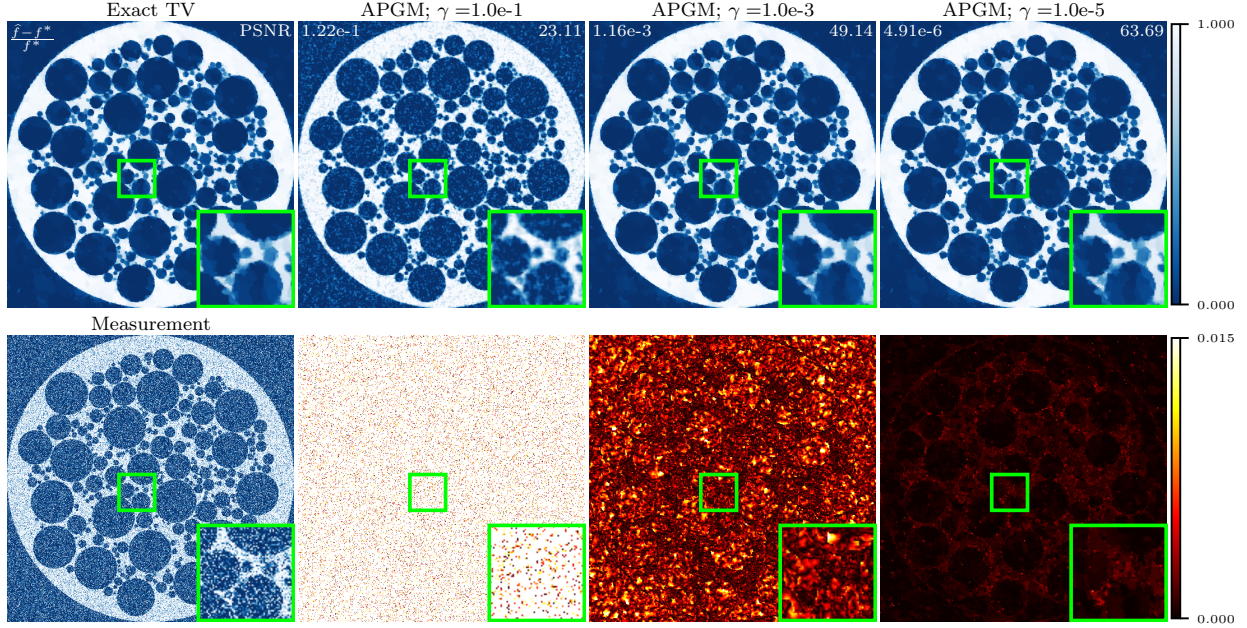


Figure 1: Effect of τ on image denoising performance when using $\mathcal{S}_\tau(\mathbf{z})$ in APGM compared to the exact TV reconstruction with regularization $\lambda = 0.5$. As written in Algorithm 1, $\tau = \gamma\lambda$, where γ is the step-size. The top-left shows the relative cost of the approximate TV reconstruction to the exact TV reconstruction. The PSNR and difference images are relative to the exact TV reconstruction. Following Proposition 2, a smaller τ results in a smaller error.

where \mathcal{T}_λ is an operator with the parameter $\lambda := \tau 2\sqrt{d} > 0$, corresponding to the application of component-wise shrinkage functions on the scaled difference components of $\mathbf{W}\mathbf{z}$. The anisotropic shrinkage function \mathcal{T}_λ^a is defined as

$$\mathcal{T}_\lambda^a(u) := \max(|u| - \lambda, 0) \frac{u}{|u|}, \quad (7)$$

where $u := 1/(2\sqrt{d})[\mathbf{D}\mathbf{z}]_j \in \mathbb{R}$ for $j \in \{1, 2, \dots, nd\}$. The isotropic shrinkage function \mathcal{T}_λ^i is defined as

$$\mathcal{T}_\lambda^i(\mathbf{u}) := \max(\|\mathbf{u}\|_2 - \lambda, 0) \frac{\mathbf{u}}{\|\mathbf{u}\|_2}, \quad (8)$$

with $\mathbf{u} := 1/(2\sqrt{d})[[\mathbf{D}_1\mathbf{z}]_i \cdots [\mathbf{D}_a\mathbf{z}]_i]^\top \in \mathbb{R}^d$ for $i \in \{1, 2, \dots, n\}$. Note that the shrinkage parameter τ must be scaled by $2\sqrt{d}$ due to the scaling of \mathbf{W} . For simplicity, we omit the superscripts a and i when we do not need to distinguish between the anisotropic and isotropic thresholding functions, and the corresponding TV functions. The following results apply to both versions.

3.2 Theoretical Analysis

We now present the theoretical analysis $\mathcal{S}_\tau(\mathbf{z})$ as an approximation of the TV proximal operator. The detailed proofs are provided in the Appendix 6.

Proposition 1. *For $\tau > 0$, there exists a proper, closed, and convex function \hat{h} such that $\mathcal{S}_\tau(\mathbf{z}) = \text{prox}_{\hat{h}}(\mathbf{z})$ for all $\mathbf{z} \in \mathbb{R}^n$.*

Proposition 1 establishes the existence of a function \widehat{h} for which $\mathcal{S}_\tau(\mathbf{z})$ is the proximal operator. Although the explicit form of \widehat{h} is unknown, its existence implies that $\mathcal{S}_\tau(\mathbf{z})$ can be incorporated into any proximal optimization method with the expectation of algorithm convergence.

We will next demonstrate that \widehat{h} provides a close approximation of h . To effectively describe the operator as an approximation of the true proximal operator for h , we introduce the concept of the subdifferential [55,56].

Definition 1. *The subdifferential of the convex function $f : \mathbb{R}^n \rightarrow (-\infty, +\infty]$ at $\mathbf{y} \in \text{dom}(f)$ is defined to be*

$$\partial f(\mathbf{y}) := \{\mathbf{g} \in \mathbb{R}^n : f(\mathbf{x}) \geq f(\mathbf{y}) + \mathbf{g}^\top(\mathbf{x} - \mathbf{y}), \forall \mathbf{x} \in \mathbb{R}^n\}.$$

A relaxation of this definition is called the ϵ -subdifferential [57] and defined as

Definition 2. *The ϵ -subdifferential of the convex function $f : \mathbb{R}^n \rightarrow (-\infty, +\infty]$ at $\mathbf{y} \in \text{dom}(f)$ is defined to be*

$$\partial_\epsilon f(\mathbf{y}) := \{\mathbf{g} \in \mathbb{R}^n : f(\mathbf{x}) \geq f(\mathbf{y}) + \mathbf{g}^\top(\mathbf{x} - \mathbf{y}) - \epsilon, \forall \mathbf{x} \in \mathbb{R}^n\}.$$

By comparing Definition 2 to Definition 1, it becomes evident that the traditional subdifferential is a subset of the ϵ -subdifferential. The ϵ -subdifferential represents the subdifferentials relaxed by ϵ .

Substantial work has been done to define and analyze various notions of approximate proximal operators [43, 48, 50, 51]. In Proposition 2, we prove that the operator $\mathcal{S}_\tau(\mathbf{z})$ can be characterized using several of the common definitions for an approximate proximal operator [48].

Proposition 2. *For all $\mathbf{z} \in \mathbb{R}^n$, the operator $\mathcal{S}_\tau(\mathbf{z})$ satisfies*

- (a) $h(\mathcal{S}_\tau(\mathbf{z})) \leq h(\mathbf{z})$ for h defined in Eq. (3) and (4),
- (b) $\mathcal{S}_\tau(\mathbf{z}) = \text{prox}_{\tau h}(\mathbf{z} + \boldsymbol{\delta})$, where $\|\boldsymbol{\delta}\|_2 \leq \tau\epsilon_1$,
- (c) $\mathbf{z} - \mathcal{S}_\tau(\mathbf{z}) \in \tau\partial_{\tau\epsilon_2} h(\mathcal{S}_\tau(\mathbf{z}))$,

where ϵ_1 and ϵ_2 are constants.

Proposition 2 (b) and 2 (c) rely on notions of approximate proximal operators, commonly used in the literature. Specifically, Proposition 2 (b) aligns with a “type 3 approximation” in the proximal operator with $\tau\epsilon_1$ -precision, while Proposition 2 (c) corresponds to a “type 2 approximation” with $\tau\sqrt{2\epsilon_2}$ -precision [48].

Proposition 2 (a) indicates that the operator decreases the TV function, meaning $\mathcal{S}_\tau(\mathbf{z})$ serves as a valid descent direction for TV. However, it does not necessarily provide the optimal descent direction that would be obtained from the true proximal operator of h . The second part of Proposition 2 demonstrates that the operator functions as a perturbed proximal operator of TV. Specifically, the output of the operator is equivalent to applying the true proximal operator of TV to a perturbed input vector \mathbf{z} , modified by a vector $\boldsymbol{\delta}$. Notably, the norm of the perturbation $\|\boldsymbol{\delta}\|_2$ is bounded and can be controlled by adjusting τ . From the optimality condition for the proximal operator of true TV regularizer $\text{prox}_{\tau h}(\mathbf{z})$, there is the following well known relationship

$$\mathbf{z} - \text{prox}_{\tau h}(\mathbf{z}) \in \tau\partial h(\text{prox}_{\tau h}(\mathbf{z})).$$

The third part of Proposition 2 establishes an analogous connection for the closed-form approximate operator, characterized using the ϵ -subdifferential from Definition 2, where ϵ is controlled by the proximal scaling parameter τ .

Overall, Proposition 2 implies that the \widehat{h} from Proposition 1 can be seen as an approximation of the true TV function h with controllable accuracy. Notably, by reducing τ , one can achieve an arbitrarily close approximation to the true TV proximal operator. Therefore, our theoretical result supports the use of $\mathcal{S}_\tau(\mathbf{z})$ as an approximation of $\text{prox}_{\tau h}(\mathbf{z})$.

Corollary 1. *For any $\tau > 0$ and for any $\mathbf{z} \in \mathbb{R}^n$*

$$\|\text{prox}_{\tau h}(\mathbf{z}) - \mathcal{S}_\tau(\mathbf{z})\|_2 \leq \tau\epsilon_1.$$

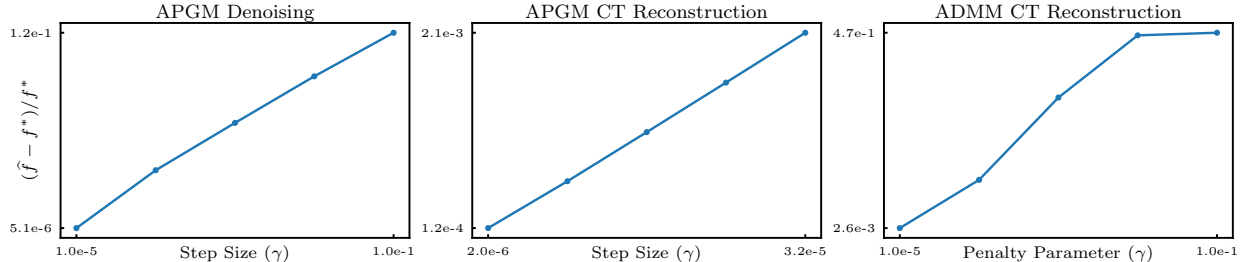


Figure 2: Effect of τ on the approximate reconstruction performance \hat{f} using the $\mathcal{S}_\tau(\mathbf{z})$ relative to the exact TV reconstruction f^* . $\mathcal{S}_\tau(\mathbf{z})$ is tested within the APGM and ADMM algorithms. For image denoising $\lambda = 0.5$ and for CT reconstruction $\lambda = 5$. In both cases, as written in Algorithms 1 and 2, $\tau = \gamma\lambda$, where γ is the step-size in APGM and the penalty parameter in ADMM. As expected from Proposition 2, the smaller the τ , the smaller the error.

Corollary 1 states that the ℓ_2 difference between the true TV proximal operator and the approximate operator $\mathcal{S}_\tau(\mathbf{z})$ has a bounded distance. As the accuracy of the operator is controlled by τ , it might initially appear that it would only be effective for problems with a very small regularization parameter λ for TV. However, this is not the case when $\mathcal{S}_\tau(\mathbf{z})$ is used within iterative algorithms such as APGM and ADMM. As shown in Algorithms 1 and 2, the shrinkage parameter for $\mathcal{S}_\tau(\mathbf{z})$ is set by $\tau = \gamma\lambda$. Thus, one can enhance accuracy by adjusting γ rather than altering the TV regularization parameter λ . For APGM, γ represents the step size, while for ADMM, γ serves as the penalty parameter in the augmented Lagrangian.

4 Numerical Validation

In this section, we numerically validate Proposition 2 by comparing the reconstruction performance of iterative proximal algorithms when $\mathcal{S}_\tau(\mathbf{z})$ replaces the true proximal operator. Specifically, we run APGM and ADMM on a simulated low-angle computed tomography (CT) image reconstruction problem. The APGM and ADMM algorithms using $\mathcal{S}_\tau(\mathbf{z})$ instead of the true proximal operator are shown in Algorithms 1 and 2, respectively. The accuracy of $\mathcal{S}_\tau(\mathbf{z})$ can be directly controlled by γ since $\tau = \gamma\lambda$, where γ is the step size and penalty parameter, for APGM and ADMM algorithms, respectively. To calculate the true proximal operator, we use the iterative Fast Projected Gradient (FPG) algorithm [5]. Additionally, we investigate the performance of the closed-form approximate operator relative to true proximal operator of TV for an image denoising task. The numerical evaluations are performed using 10 piecewise-smooth foam phantoms generated by the XDesign Python package [58] and the implementations of $\mathcal{S}_\tau(\mathbf{z})$ in the SCICO Python package [59]. All algorithms are run until the stopping criteria

$$\frac{\|\mathbf{x}^t - \mathbf{x}^{t-1}\|_2}{\|\mathbf{x}^{t-1}\|_2} \leq 5 \times 10^{-6} \quad (9)$$

is met.

4.1 Image Denoising

In the case of image denoising, the forward model is $\mathbf{A} = \mathbf{I}$, which results in the data-fidelity term $g(\mathbf{x}) = \frac{1}{2}\|\mathbf{y} - \mathbf{x}\|_2^2$. We report the denoising results for the regularization parameters 0.25, 0.5, and 1 in Table 1. Since FPG solves the denoising problem, it is directly used to compute the exact TV regularized denoised image. The APGM algorithm with $\mathcal{S}_\tau(\mathbf{z})$ is used to compute the approximate TV regularized images.

See classes AnisotropicTVNorm and IsotropicTVNorm.

Table 1: The relative cost, PSNR with respect to the exact TV solution and groundtruth for various regularization (λ) and step-size/penalty (γ) parameters for image denoising and CT reconstruction. For the APGM and ADMM algorithms, $\tau = \gamma\lambda$, where γ determines the accuracy of $\mathcal{S}_\tau(\mathbf{z})$. The metrics have been averaged across the 10 images in the dataset. Note that L is the Lipschitz constant of ∇g .

APGM Image Denoising												
Step Size (γ)	$\lambda = 0.25$			$\lambda = 0.5$			$\lambda = 1$					
	Cost	Acc.	PSNR (TV)	PSNR (GT)	Cost	Acc.	PSNR (TV)	PSNR (GT)	Cost	Acc.	PSNR (TV)	PSNR (GT)
1e-1	1.751e-02		31.97	16.44	1.214e-01		23.14	17.57	3.875e-01		19.65	17.38
1e-2	1.364e-03		48.02	16.72	1.281e-02		34.52	18.57	5.467e-02		25.82	15.68
1e-3	1.152e-04		65.90	16.72	1.157e-03		49.16	18.75	5.945e-03		36.31	15.96

APGM CT Reconstruction												
Step Size (γ)	$\lambda = 2.5$			$\lambda = 5$			$\lambda = 10$					
	Cost	Acc.	PSNR (TV)	PSNR (GT)	Cost	Acc.	PSNR (TV)	PSNR (GT)	Cost	Acc.	PSNR (TV)	PSNR (GT)
1/(1L)	9.473e-04		57.28	21.07	2.069e-03		52.08	20.86	4.588e-03		46.48	20.41
1/(2L)	4.609e-04		59.46	21.06	1.002e-03		56.87	20.88	2.208e-03		51.84	20.48
1/(4L)	2.264e-04		62.14	21.07	4.874e-04		60.42	20.88	1.068e-03		56.79	20.51

ADMM CT Reconstruction												
Pen. Par. (γ)	$\lambda = 2.5$			$\lambda = 5$			$\lambda = 10$					
	Cost	Acc.	PSNR (TV)	PSNR (GT)	Cost	Acc.	PSNR (TV)	PSNR (GT)	Cost	Acc.	PSNR (TV)	PSNR (GT)
1e-2	3.545e-01		18.49	15.35	4.341e-01		18.10	15.13	4.680e-01		18.28	15.13
1e-3	3.767e-02		31.63	19.82	8.291e-02		26.42	18.59	1.788e-01		21.91	16.82
1e-4	4.850e-03		40.42	20.59	9.284e-03		38.55	20.37	1.989e-02		35.13	19.82

4.2 Computed Tomography

We validate the application of $\mathcal{S}_\tau(\mathbf{z})$ for the limited-angle computed tomography (CT) reconstruction. The data fidelity term in Eq. (2) is $g(\mathbf{x}) = \frac{1}{2}\|\mathbf{Ax} - \mathbf{y}\|_2^2$, where \mathbf{A} represents the CT imaging forward operator using only 45 angles, resulting in an ill-posed inverse problem. We show the experimental results for the regularization parameters λ corresponding to 2.5, 5, and 10, using both APGM and ADMM. ADMM is implemented to solve the constrained optimization problem

$$\arg \min_{\mathbf{x}, \mathbf{z}} g(\mathbf{x}) + \lambda h(\mathbf{z}) \quad \text{s.t.} \quad \mathbf{z} = \mathbf{x}$$

in order to test the impact of $\mathcal{S}_\tau(\mathbf{z})$. The exact TV reconstruction is obtained by running 50 sub-iterations of FPG to calculate the exact proximal within both algorithms.

4.3 Discussion

According to Proposition 1, $\mathcal{S}_\tau(\mathbf{z})$ serves as the proximal operator for some convex function. Consequently, the iterates of a proximal-based reconstruction algorithm a convex function are expected to converge. Activation of the termination criteria in 9 occurs for all the experiments, validating the convergence of the algorithms under $\mathcal{S}_\tau(\mathbf{z})$.

The statements in Proposition 2 and Corollary 1 imply smaller τ in $\mathcal{S}_\tau(\mathbf{z})$ provides a better approximation with respect to the true TV reconstruction. This relationship is experimentally validated in Table 1 across all experiments: a smaller τ results in a smaller relative error in the approximate reconstruction loss \hat{f} , compared to the true TV reconstruction loss f^* . Similarly, the PSNR with respect to the true TV reconstruction increases as τ decreases, suggesting $\mathcal{S}_\tau(\mathbf{z})$ provides a better approximation of the TV proximal operator. Figure 2 illustrates the dependence of cost accuracy on parameter γ for image denoising with $\lambda = 0.5$ and CT image reconstruction with $\lambda = 5$. Figures 1, 3, and 4 illustrate visual comparison for image denoising and CT reconstruction using true TV proximal and $\mathcal{S}_\tau(\mathbf{z})$ operator with various γ . The visual results indicate that

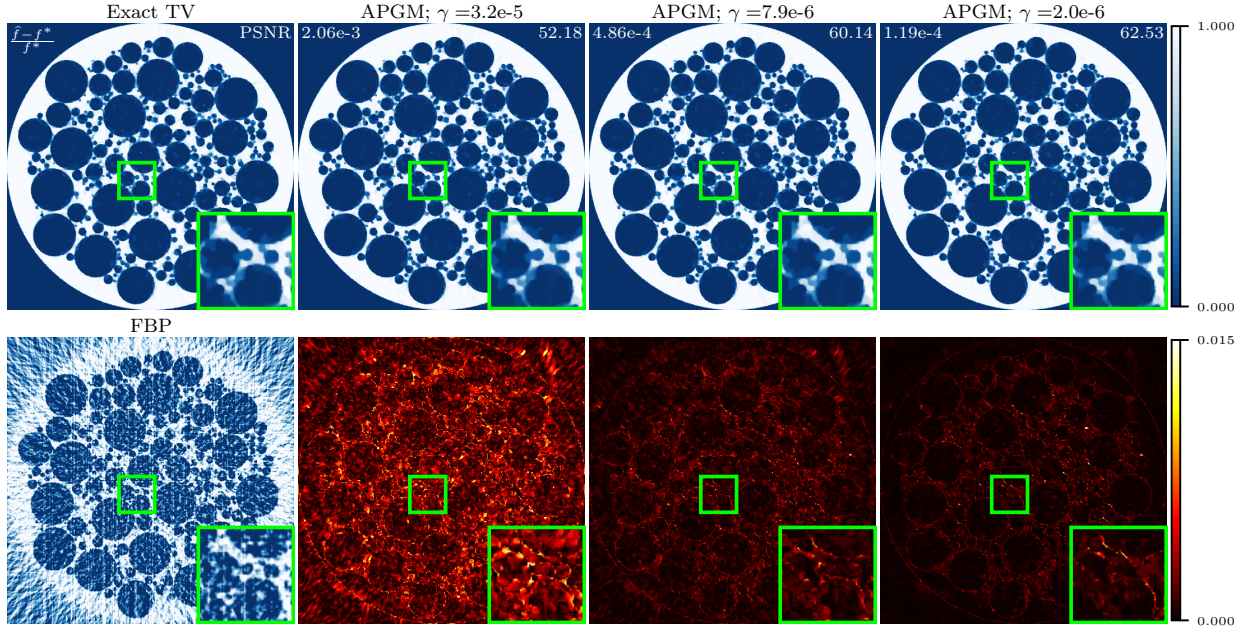


Figure 3: Effect of τ on limited angle Computed Tomography (CT) reconstruction using $\mathcal{S}_\tau(z)$ in APGM compared to the exact TV reconstruction with regularization $\lambda = 5$. As written in Algorithm 1, $\tau = \gamma\lambda$, where γ is the step-size. The top-left shows relative cost of the approximate reconstruction to the exact reconstruction. The PSNR and difference images are relative to the exact reconstruction. Following Proposition 2, a smaller τ results in a smaller error.

$\mathcal{S}_\tau(z)$ promotes piecewise smooth images, as is expected from an approximate TV proximal operator. Both visual and numerical results from the experiments support the theoretical finding presented in Section 3.2, demonstrating that $\mathcal{S}_\tau(z)$ can approximate the TV proximal and be effectively integrated into proximal-based iterative algorithms to achieve approximate TV-regularized reconstructions.

5 Conclusion

We theoretically analyzed a closed-form operator that approximates the proximal operator for both anisotropic and isotropic total variation. While these operators have been previously explored in the context of optimization algorithms, this work focuses on the operator itself. Specifically, we demonstrated that the operator consistently reduces the TV function of the input signal and that its error, relative to the true TV proximal operator, can be characterized using well-established notions of approximate proximal operators. Through this analysis, we provide a foundation for employing $\mathcal{S}_\tau(z)$ within any proximal-based reconstruction method to address TV-regularized imaging inverse problems. Finally, we supported our theoretical findings with several experiments.

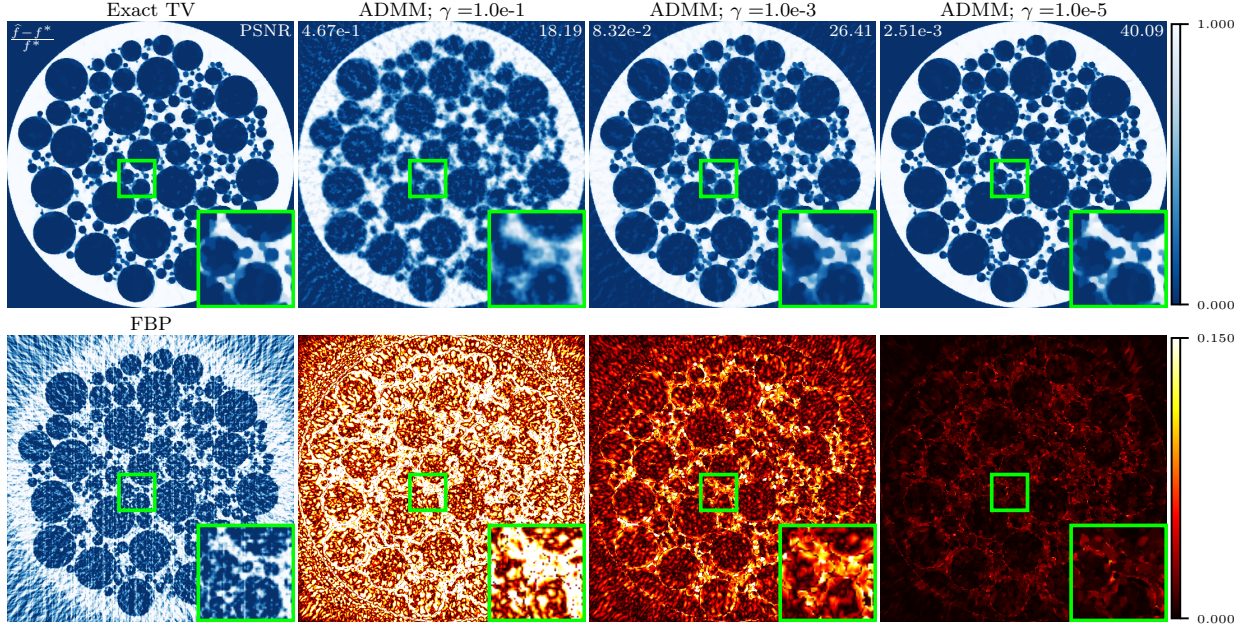


Figure 4: Effect of τ on limited angle Computed Tomography (CT) reconstruction using $\mathcal{S}_\tau(\mathbf{z})$ in ADMM compared to exact reconstruction with regularization $\lambda = 5$. As written in Algorithm 2, $\tau = \gamma\lambda$, where γ is the penalty parameter. The top-left shows relative cost of the approximate reconstruction to the exact reconstruction. The PSNR and difference images are relative to exact reconstruction. Following Proposition 2, a smaller τ results in a smaller error.

6 Appendix

In this section, we will prove Propositions 1, 2, and Corollary 1. First, we define the function $\bar{h} : \mathbb{R}^{2nd} \rightarrow \mathbb{R}$, where \bar{h} has an anisotropic and isotropic form, \bar{h}^a and \bar{h}^i , respectively. For $\mathbf{u} \in \mathbb{R}^{2nd}$,

$$\bar{h}^a(\mathbf{u}) := 2\sqrt{d}\|\mathbf{u}^{\text{dif}}\|_{1,1} = 2\sqrt{d}\sum_{i=1}^n \|[\mathbf{u}^{\text{dif}}]_i\|_1 \quad (10)$$

$$\bar{h}^i(\mathbf{u}) := 2\sqrt{d}\|\mathbf{u}^{\text{dif}}\|_{2,1} = 2\sqrt{d}\sum_{i=1}^n \|[\mathbf{u}^{\text{dif}}]_i\|_2, \quad (11)$$

where $\mathbf{u}^{\text{dif}} \in \mathbb{R}^{nd}$ denotes the difference coefficients. $\|\mathbf{u}^{\text{dif}}\|_{p,1}$ is a group norm, where p is either 1 or 2, corresponding to anisotropic and isotropic TV, respectively. The grouping is based on the d elements that represent the discrete differences at a specific location for each of the d dimensions, with the p -norm applied within each group. Each $[\mathbf{u}^{\text{dif}}]_i \in \mathbb{R}^d$ is the vector of discrete differences at location i . We see

$$\bar{h}(\mathbf{u}) := 2\sqrt{d}\|\mathbf{u}^{\text{dif}}\|_{p,1} \quad (12)$$

to refer to both the anisotropic and isotropic versions. Thus the results in Proposition 1 and Proposition 2 hold for both anisotropic and isotropic versions. We can also rewrite the TV definitions in Eq. (3) and Eq. (4) in the general form

$$h(\mathbf{z}) = \|\mathbf{D}\mathbf{z}\|_{p,1}. \quad (13)$$

The term $2\sqrt{d}$ in front of \bar{h} is necessary so that the relationship

$$\bar{h}(\mathbf{W}\mathbf{z}) = h(\mathbf{z}) \quad (14)$$

holds. Note that Eq. (14) implies that for $\mathbf{z} \in \mathbb{R}^n$, \bar{h} evaluated at $\mathbf{W}\mathbf{z}$ is equivalent to h evaluated at \mathbf{z} ; however, \bar{h} is not the TV function itself since it is defined on the entire \mathbb{R}^{2nd} , and not \mathbb{R}^n .

Additionally, \bar{h} is defined as the scaled version of two well-known norms that are proper, closed, and convex. By using the notation Γ^0 to represent the set of proper, closed, and convex functions, we have $\bar{h} \in \Gamma^0(\mathbb{R}^{2nd})$. Finally, define the linear subspace $\mathcal{U} := \{\mathbf{u} \mid \mathbf{u} = \mathbf{W}\mathbf{W}^\top \mathbf{u}\} \subset \mathbb{R}^{2nd}$.

Proof of Proposition 1

Proposition 1. *For $\tau > 0$, there exists $\hat{h} \in \Gamma^0(\mathbb{R}^n)$ such that $\mathcal{S}_\tau(\mathbf{z}) = \text{prox}_{\hat{h}}(\mathbf{z})$ for all $\mathbf{z} \in \mathbb{R}^n$.*

Proof. To establish that $\mathcal{S}_\tau(\mathbf{z})$ is a proximal operator of some $\hat{h} \in \Gamma^0(\mathbb{R}^n)$, it is sufficient to show that

1. There exists a closed and convex ψ such that $\mathcal{S}_\tau(\mathbf{z}) \in \partial\psi(\mathbf{z})$, $\forall \mathbf{z} \in \mathbb{R}^n$.
2. The operator $\mathcal{S}_\tau(\mathbf{z})$ is nonexpansive.

This equivalence was given in Corollary 10.c in [55]. As defined in Eq. (12), \bar{h} is the scaled norm of the difference components of its input vector in \mathbb{R}^{2nd} . Therefore, the proximal operator of $\tau\bar{h}(\mathbf{u})$ can be written using the thresholding function defined in Eq. (7) and Eq. (8):

$$\text{prox}_{\tau\bar{h}}(\mathbf{u}) = \mathcal{T}_{\tau 2\sqrt{d}}(\mathbf{u}) \quad \forall \mathbf{u} \in \mathbb{R}^{2nd}. \quad (15)$$

By Corollary 10.c in [55], there exists a closed and convex ϕ such that $\mathcal{T}_{\tau 2\sqrt{d}}(\mathbf{u}) \in \partial\phi(\mathbf{u})$. Plugging in $\mathbf{u} = \mathbf{W}\mathbf{z}$ and multiplying both sides by \mathbf{W}^\top gives us $\mathcal{S}_\tau(\mathbf{z}) \in \mathbf{W}^\top \partial\phi(\mathbf{W}\mathbf{z})$. By the subdifferential chain rule, we know that $\mathbf{W}^\top \partial\phi(\mathbf{W}\mathbf{z}) \subset \partial[\phi \circ \mathbf{W}](\mathbf{z})$, where \circ denotes composition of the functions. Therefore, we have

$$\mathcal{S}_\tau(\mathbf{z}) \in \partial[\phi \circ \mathbf{W}](\mathbf{z}).$$

Next, letting $\psi(\mathbf{z}) = [\phi \circ \mathbf{W}](\mathbf{z})$, we need to show ψ is closed and convex. Since ϕ is closed, $\phi \circ \mathbf{W}$ is also closed. To show convexity, letting $\mathbf{z}_1, \mathbf{z}_2 \in \mathbb{R}^n$,

$$\begin{aligned} \psi(\alpha\mathbf{z}_1 + (1-\alpha)\mathbf{z}_2) &= [\phi \circ \mathbf{W}](\alpha\mathbf{z}_1 + (1-\alpha)\mathbf{z}_2) \\ &= \phi(\alpha\mathbf{W}\mathbf{z}_1 + (1-\alpha)\mathbf{W}\mathbf{z}_2) \\ &\leq \alpha\phi(\mathbf{W}\mathbf{z}_1) + (1-\alpha)\phi(\mathbf{W}\mathbf{z}_2) \\ &= \alpha\psi(\mathbf{z}_1) + (1-\alpha)\psi(\mathbf{z}_2), \end{aligned} \quad (16)$$

where the inequality comes from convexity of ϕ . By definition of convexity, ψ is thus convex. We can show $\|\mathbf{W}\|_2 = 1$ as follows

$$\begin{aligned} \|\mathbf{W}\|_2 &= \sqrt{\sigma_{\max}(\mathbf{W}^\top \mathbf{W})} \\ &= \sqrt{\sigma_{\max}(\mathbf{I})} = 1, \end{aligned} \quad (17)$$

where $\sigma_{\max}(\mathbf{I})$ is the largest eigenvalue of \mathbf{I} .

We now verify the nonexpansiveness of $\mathcal{S}_\tau(\mathbf{z})$.

$$\begin{aligned}
& \|\mathcal{S}_\tau(\mathbf{z}_1) - \mathcal{S}_\tau(\mathbf{z}_2)\|_2 \\
&= \|\mathbf{W}^\top \mathcal{T}_{\tau 2\sqrt{d}}(\mathbf{W}\mathbf{z}_1) - \mathbf{W}^\top \mathcal{T}_{\tau 2\sqrt{d}}(\mathbf{W}\mathbf{z}_2)\|_2 \\
&= \|\mathbf{W}^\top (\mathcal{T}_{\tau 2\sqrt{d}}(\mathbf{W}\mathbf{z}_1) - \mathcal{T}_{\tau 2\sqrt{d}}(\mathbf{W}\mathbf{z}_2))\|_2 \\
&\leq \|\mathbf{W}^\top\|_2 \|\mathcal{T}_{\tau 2\sqrt{d}}(\mathbf{W}\mathbf{z}_1) - \mathcal{T}_{\tau 2\sqrt{d}}(\mathbf{W}\mathbf{z}_2)\|_2 \\
&= \|\mathcal{T}_{\tau 2\sqrt{d}}(\mathbf{W}\mathbf{z}_1) - \mathcal{T}_{\tau 2\sqrt{d}}(\mathbf{W}\mathbf{z}_2)\|_2 \\
&\leq \|\mathbf{W}\mathbf{z}_1 - \mathbf{W}\mathbf{z}_2\|_2 \\
&\leq \|\mathbf{W}\|_2 \|\mathbf{z}_1 - \mathbf{z}_2\|_2 \\
&= \|\mathbf{z}_1 - \mathbf{z}_2\|_2,
\end{aligned}$$

Where the third and last equalities comes from Eq. (17). The second inequality comes from the fact that soft-thresholding is a non-expansive operator. The above inequality is exactly the definition of a nonexpansive operator. \square

Proof of Proposition 2

Proposition 2. For all $\mathbf{z} \in \mathbb{R}^n$, the operator $\mathcal{S}_\tau(\mathbf{z})$ satisfies

- (a) $h(\mathcal{S}_\tau(\mathbf{z})) \leq h(\mathbf{z})$ for h defined in Eq. (3) and Eq. (4),
- (b) $\mathcal{S}_\tau(\mathbf{z}) = \text{prox}_{\tau h}(\mathbf{z} + \boldsymbol{\delta})$ where $\|\boldsymbol{\delta}\| \leq \tau\epsilon_1$,
- (c) $\mathbf{z} - \mathcal{S}_\tau(\mathbf{z}) \in \tau\partial_{\tau\epsilon_2} h(\mathcal{S}_\tau(\mathbf{z}))$,

where ϵ_1 and ϵ_2 are constants.

Proof. Proof of Part (a). By using the definition of TV in Eq. (13) we obtain

$$\begin{aligned}
h(\mathcal{S}_\tau(\mathbf{z})) &= \|\mathbf{D}\mathcal{S}_\tau(\mathbf{z})\|_{p,1} \\
&= \|\mathbf{D}(\mathbf{W}^\top \mathcal{T}_{\tau 2\sqrt{d}}(\mathbf{W}\mathbf{z}))\|_{p,1} \\
&= 2\sqrt{d} \|[\mathbf{W}(\mathbf{W}^\top \mathcal{T}_{\tau 2\sqrt{d}}(\mathbf{W}\mathbf{z}))]^{\text{dif}}\|_{p,1},
\end{aligned}$$

where we used the definition of the operator $\mathcal{S}_\tau(\mathbf{z})$ in the second line. In the last line, we used the fact that \mathbf{W} includes difference operator \mathbf{D} scaled by $2\sqrt{d}$ (that is, $\mathbf{W} := (1/2\sqrt{d})[\mathbf{A} \ \mathbf{D}]^\top$).

The thresholding operator $\mathcal{T}_{\tau 2\sqrt{d}}$ reduces the magnitude of each difference component by multiplying it by some value in $(0, 1)$. Each average component remains the same. Thus, $[\mathbf{W}\mathbf{z}]_i$ is multiplied by α_i , where $0 < \alpha_i \leq 1$. Therefore, we can replace $\mathbf{W}\mathbf{W}^\top$ with the vector $\boldsymbol{\alpha} \in \mathbb{R}^{2nd}$ where each α_i satisfies $0 \leq \alpha_i \leq 1$. Here, \odot signifying component-wise multiplication. Consequently, we have

$$\begin{aligned}
h(\mathcal{S}_\tau(\mathbf{z})) &= 2\sqrt{d} \|[\mathbf{W}\mathbf{W}^\top(\boldsymbol{\alpha} \odot (\mathbf{W}\mathbf{z}))]^{\text{dif}}\|_{p,1} \\
&= 2\sqrt{d} \|[\boldsymbol{\alpha}]^{\text{dif}} \odot [\mathbf{W}\mathbf{W}^\top \mathbf{W}\mathbf{z}]^{\text{dif}}\|_{p,1} \\
&\leq 2\sqrt{d} \|[\mathbf{W}\mathbf{z}]^{\text{dif}}\|_{p,1} \\
&= \|\mathbf{D}\mathbf{z}\|_{p,1} = h(\mathbf{z}).
\end{aligned}$$

Component-wise multiplication is commutative, allowing us to swap $\boldsymbol{\alpha}$ and $\mathbf{W}\mathbf{W}^\top$ in the second equality. The inequality comes from $\mathbf{W}^\top \mathbf{W} = \mathbf{I}$ and the fact that each α_i satisfies $0 \leq \alpha_i \leq 1$. This establishes the desired result of part (a).

Proof of Part (b). We know $\|\mathbf{W}\|_2 = 1$ from (17). For both the anisotropic and isotropic versions, by its definition the soft-thresholding operator $\mathcal{T}_{\tau 2\sqrt{d}}(\mathbf{W}\mathbf{z})$ at most changes each of the nd difference elements of $\mathbf{W}\mathbf{z}$ by $2\tau\sqrt{d}$, so we can bound

$$\begin{aligned}\|\mathcal{T}_{\tau 2\sqrt{d}}(\mathbf{W}\mathbf{z}) - \mathbf{W}\mathbf{z}\|_2 &\leq \sqrt{nd(2\tau\sqrt{d})^2} \\ &= \sqrt{4\tau^2 nd^2} \\ &= 2\tau d\sqrt{n}.\end{aligned}\tag{18}$$

We bound $\|\mathcal{S}_\tau(\mathbf{z}) - \mathbf{z}\|_2$ by Eq. (17) and Eq. (18)

$$\begin{aligned}\|\mathcal{S}_\tau(\mathbf{z}) - \mathbf{z}\|_2 &= \|\mathcal{S}_\tau(\mathbf{z}) - \mathbf{W}^\top \mathbf{W}\mathbf{z}\|_2 \\ &\leq \|\mathcal{T}_{\tau 2\sqrt{d}}(\mathbf{W}\mathbf{z}) - \mathbf{W}\mathbf{z}\|_2 \\ &\leq 2\tau d\sqrt{n}.\end{aligned}\tag{19}$$

For $\Phi_\tau(\mathbf{y}) := \frac{1}{2\tau}\|\mathbf{y} - \mathbf{z}\|_2^2 + h(\mathbf{y})$, its subdifferential at $\mathcal{S}_\tau(\mathbf{z})$ is

$$\begin{aligned}\partial\Phi_\tau(\mathcal{S}_\tau(\mathbf{z})) &= \frac{1}{\tau}(\mathcal{S}_\tau(\mathbf{z}) - \mathbf{z}) + \partial h(\mathcal{S}_\tau(\mathbf{z})) \\ &= \frac{1}{\tau}(\mathcal{S}_\tau(\mathbf{z}) - \mathbf{z}) + \partial[\bar{h} \circ \mathbf{W}](\mathcal{S}_\tau(\mathbf{z})) \\ &= \frac{1}{\tau}(\mathcal{S}_\tau(\mathbf{z}) - \mathbf{z}) + \mathbf{W}^\top \partial\bar{h}(\mathbf{W}\mathcal{S}_\tau(\mathbf{z})),\end{aligned}$$

where the second equality comes from $\bar{h} \circ \mathbf{W} = h$ and the third equality comes from the chain rule.

The distance $d(\mathbf{0}, \partial\Phi_\tau(\mathcal{S}_\tau(\mathbf{z})))$ is defined as the minimum ℓ_2 distance between $\mathbf{0}$ and any vector in $\partial\Phi_\tau(\mathcal{S}_\tau(\mathbf{z}))$. Therefore, letting $\mathbf{g}_1 \in \partial\bar{h}(\mathbf{W}\mathcal{S}_\tau(\mathbf{z}))$, we get the following inequality

$$\begin{aligned}d(\mathbf{0}, \partial\Phi_\tau(\mathcal{S}_\tau(\mathbf{z}))) &\leq \left\| \mathbf{0} - \left(\frac{1}{\tau}(\mathcal{S}_\tau(\mathbf{z}) - \mathbf{z}) + \mathbf{W}^\top \mathbf{g}_1 \right) \right\|_2 \\ &\leq \frac{1}{\tau} \|\mathcal{S}_\tau(\mathbf{z}) - \mathbf{z}\|_2 + \|\mathbf{W}^\top \mathbf{g}_1\|_2 \\ &\leq \frac{1}{\tau} (2\tau d\sqrt{n}) + \|\mathbf{g}_1\|_2 \\ &\leq \frac{1}{\tau} (2\tau d\sqrt{n}) + 2d\sqrt{n} = \frac{\tau\epsilon_1}{\tau},\end{aligned}\tag{20}$$

with $\epsilon_1 = 4d\sqrt{n}$. The third inequality comes from (19) and nonexpansiveness of \mathbf{W}^\top . The fourth inequality comes from the fact that the norm of any gradient of \bar{h} is bounded by $2d\sqrt{n}$, as shown in Lemma 1.

Letting $\mathbf{g}_2 \in \partial\Phi_\tau(\mathcal{S}_\tau(\mathbf{z}))$, we can write $\|\mathbf{g}_2\| \leq \frac{\tau\epsilon_1}{\tau}$. Equivalently,

$$\begin{aligned}\mathbf{g}_2 &\in \frac{1}{\tau}(\mathcal{S}_\tau(\mathbf{z}) - \mathbf{z}) + \partial h(\mathcal{S}_\tau(\mathbf{z})) \\ &\iff \\ \mathbf{z} + \boldsymbol{\delta} - \mathcal{S}_\tau(\mathbf{z}) &\in \tau \partial h(\mathcal{S}_\tau(\mathbf{z})) \\ &\iff \\ \mathcal{S}_\tau(\mathbf{z}) &= \text{prox}_{\tau h}(\mathbf{z} + \boldsymbol{\delta}), \text{ where } \|\boldsymbol{\delta}\|_2 \leq \tau\epsilon_1,\end{aligned}$$

and $\boldsymbol{\delta} = \tau\mathbf{g}_2$. The last equivalence comes from the property of proximal operators that $\mathbf{x} = \text{prox}_{\tau h}(\mathbf{y}) \iff \mathbf{y} - \mathbf{x} \in \tau \partial h(\mathbf{x})$. This establishes the desired result of part (b).

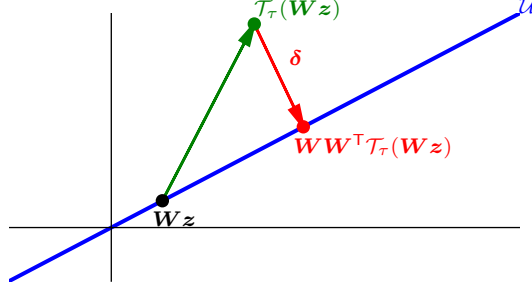


Figure 5: A visual illustration of the characterization of the projection as $\mathbf{W}\mathbf{W}^\top \mathcal{T}_{\tau 2\sqrt{d}}(\mathbf{W}\mathbf{z}) = \mathcal{T}_{\tau 2\sqrt{d}}(\mathbf{W}\mathbf{z}) + \boldsymbol{\delta}$. For any $\mathbf{z} \in \mathbb{R}^n$, the vector $\mathbf{W}\mathbf{z} \in \mathcal{U} := \{\mathbf{u} \mid \mathbf{u} = \mathbf{W}\mathbf{W}^\top \mathbf{u}\}$. Applying the soft-thresholding function gives $\mathcal{T}_{\tau 2\sqrt{d}}(\mathbf{W}\mathbf{z})$, not necessarily in \mathcal{U} . Applying $\mathbf{W}\mathbf{W}^\top$ projects back to \mathcal{U} , which can be represented as $\mathcal{T}_{\tau 2\sqrt{d}}(\mathbf{W}\mathbf{z}) + \boldsymbol{\delta}$.

Proof of Part (c). From the definition of the subgradient and the proximal operator, we have

$$\mathbf{u} = \text{prox}_{\tau \bar{h}}(\mathbf{W}\mathbf{z}) \iff \mathbf{W}\mathbf{z} - \mathbf{u} \in \tau \partial \bar{h}(\mathbf{u}).$$

By definition of subgradient, $\forall \mathbf{w} \in \mathbb{R}^{2nd}$

$$\bar{h}(\mathbf{w}) \geq \bar{h}(\mathbf{u}) + \left(\frac{\mathbf{W}\mathbf{z} - \mathbf{u}}{\tau} \right)^\top (\mathbf{w} - \mathbf{u}).$$

By replacing \mathbf{w} with $\mathbf{W}\mathbf{y}$, where $\mathbf{y} \in \mathbb{R}^n$, we obtain

$$\begin{aligned} \bar{h}(\mathbf{W}\mathbf{y}) &\geq \bar{h}(\mathbf{u}) + \frac{1}{\tau} (\mathbf{W}\mathbf{z} - \mathbf{u})^\top (\mathbf{W}\mathbf{y} - \mathbf{u}) \\ &= \bar{h}(\mathbf{u}) + \frac{1}{\tau} \left((\mathbf{W}\mathbf{z})^\top (\mathbf{W}\mathbf{y}) - (\mathbf{W}(z + \mathbf{y}))^\top \mathbf{u} + \|\mathbf{u}\|_2^2 \right) \\ &\geq \bar{h}(\mathbf{u}) + \frac{1}{\tau} \left(\mathbf{z}^\top \mathbf{y} - (z + \mathbf{y})^\top (\mathbf{W}^\top \mathbf{u}) + \|\mathbf{W}^\top \mathbf{u}\|_2^2 \right) \\ &= \bar{h}(\mathbf{u}) + \frac{1}{\tau} (z - \mathbf{W}^\top \mathbf{u})^\top (\mathbf{y} - \mathbf{W}^\top \mathbf{u}) \\ &= \bar{h}(\mathcal{T}_{\tau 2\sqrt{d}}(\mathbf{W}\mathbf{z})) + \frac{1}{\tau} (z - \mathcal{S}_\tau(z))^\top (\mathbf{y} - \mathcal{S}_\tau(z)), \end{aligned} \quad (21)$$

where the last inequality comes from the definition of adjoint $(\mathbf{W}\mathbf{x}_1)^\top \mathbf{x}_2 = \mathbf{x}_1^\top (\mathbf{W}^\top \mathbf{x}_2)$, the fact that $\mathbf{W}^\top \mathbf{W} = \mathbf{I}$, and that $\|\mathbf{W}^\top\|_2 = 1$. In the last line, we used the fact that $\mathbf{u} = \text{prox}_{\tau \bar{h}}(\mathbf{W}\mathbf{z}) = \mathcal{T}_{\tau 2\sqrt{d}}(\mathbf{W}\mathbf{z})$ from Eq. 15 and $\mathcal{S}_\tau(z) = \mathbf{W}^\top \mathbf{u}$.

The projection can be characterized as

$$\mathbf{W}\mathbf{W}^\top \mathcal{T}_{\tau 2\sqrt{d}}(\mathbf{W}\mathbf{z}) = \mathcal{T}_{\tau 2\sqrt{d}}(\mathbf{W}\mathbf{z}) + \boldsymbol{\delta}. \quad (22)$$

That is, $\boldsymbol{\delta}$ is the orthogonal component of $\mathcal{T}_{\tau 2\sqrt{d}}(\mathbf{W}\mathbf{z})$ to the subspace $\mathcal{U} := \{\mathbf{u} \mid \mathbf{u} = \mathbf{W}\mathbf{W}^\top \mathbf{u}\}$. Figure 5 provides a visual representation.

For both the anisotropic and isotropic versions, the soft-thresholding operator $\mathcal{T}_{\tau 2\sqrt{d}}(\mathbf{W}\mathbf{z})$ at most changes each of the nd difference elements of $\mathbf{W}\mathbf{z}$ by $2\tau\sqrt{d}$, giving the bound

$$\begin{aligned} \|\mathcal{T}_{\tau 2\sqrt{d}}(\mathbf{W}\mathbf{z}) - \mathbf{W}\mathbf{z}\|_2 &\leq \sqrt{nd(2\tau\sqrt{d})^2} \\ &= \sqrt{4\tau^2 nd^2} \\ &= 2\tau d \sqrt{n}. \end{aligned} \quad (23)$$

Since the projection $\mathbf{W}\mathbf{W}^\top$ minimizes the ℓ_2 distance between $\mathcal{T}_{\tau 2\sqrt{d}}(\mathbf{W}\mathbf{z})$ and \mathcal{U} , the following inequality holds

$$\begin{aligned}\|\boldsymbol{\delta}\|_2 &= \min_{\mathbf{w} \in \mathcal{U}} \|\mathbf{w} - \mathcal{T}_{\tau 2\sqrt{d}}(\mathbf{W}\mathbf{z})\|_2 \\ &\leq \|\mathbf{w} - \mathcal{T}_{\tau 2\sqrt{d}}(\mathbf{W}\mathbf{z})\|_2 \quad \forall \mathbf{w} \in \mathcal{U}.\end{aligned}$$

Since $\mathbf{W}\mathbf{z} \in \mathcal{U}$, this yields

$$\|\boldsymbol{\delta}\|_2 \leq \|\mathcal{T}_{\tau 2\sqrt{d}}(\mathbf{W}\mathbf{z}) - \mathbf{W}\mathbf{z}\|_2 \leq 2\tau d\sqrt{n}.$$

Furthermore,

$$\begin{aligned}\|\boldsymbol{\delta}^{\text{dif}}\|_{2,1} &\leq \|\boldsymbol{\delta}^{\text{dif}}\|_{1,1} = \|\boldsymbol{\delta}^{\text{dif}}\|_1 \\ &\leq \sqrt{nd}\|\boldsymbol{\delta}^{\text{dif}}\|_2 \\ &\leq \sqrt{nd}\|\boldsymbol{\delta}\|_2 \\ &\leq (\sqrt{nd})(2\tau d\sqrt{n}) \\ &= 2\tau nd^{3/2},\end{aligned}$$

where the first inequality comes from the fact that the ℓ_2 norm is smaller than the ℓ_1 norm for any given vector. The second inequality comes from the fact that the ℓ_1 norm is at most the square root of the dimension of the vector times its ℓ_2 norm.

Using the definition of \bar{h} in Eq. (12) relationship $\bar{h}(\mathbf{W}\mathbf{z}) = h(\mathbf{z})$, shown in Eq. (14), we get

$$\begin{aligned}h(\mathcal{S}_\tau(\mathbf{z})) &= \bar{h}(\mathbf{W}\mathcal{S}_\tau(\mathbf{z})) \\ &= 2\sqrt{d}\|[\mathbf{W}\mathcal{S}_\tau(\mathbf{z})]^{\text{dif}}\|_{p,1} \\ &= 2\sqrt{d}\|[\mathbf{W}\mathbf{W}^\top \mathcal{T}_{\tau 2\sqrt{d}}(\mathbf{W}\mathbf{z})]^{\text{dif}}\|_{p,1} \\ &= 2\sqrt{d}\|[\mathcal{T}_{\tau 2\sqrt{d}}(\mathbf{W}\mathbf{z}) + \boldsymbol{\delta}]^{\text{dif}}\|_{p,1} \\ &\leq 2\sqrt{d}\|[\mathcal{T}_{\tau 2\sqrt{d}}(\mathbf{W}\mathbf{z})]^{\text{dif}}\|_{p,1} + 2\sqrt{d}\|\boldsymbol{\delta}^{\text{dif}}\|_{p,1} \\ &\leq 2\sqrt{d}\|[\mathcal{T}_{\tau 2\sqrt{d}}(\mathbf{W}\mathbf{z})]^{\text{dif}}\|_{p,1} + (2\sqrt{d})(2\tau nd^{3/2}) \\ &= \bar{h}(\mathcal{T}_{\tau 2\sqrt{d}}(\mathbf{W}\mathbf{z})) + 4\tau nd^2.\end{aligned}$$

Rearranging the above inequality yields

$$\bar{h}(\mathcal{T}_{\tau 2\sqrt{d}}(\mathbf{W}\mathbf{z})) \geq h(\mathcal{S}_\tau(\mathbf{z})) - 4\tau nd^2. \quad (24)$$

From Eq. (21) we have

$$h(\mathbf{y}) \geq \bar{h}(\mathcal{T}_{\tau 2\sqrt{d}}(\mathbf{W}\mathbf{z})) + \frac{1}{\tau}(\mathbf{z} - \mathcal{S}_\tau(\mathbf{z}))^\top (\mathbf{y} - \mathcal{S}_\tau(\mathbf{z})).$$

Combining this with Eq. (24) provides the following for all $\mathbf{y} \in \mathbb{R}^n$

$$h(\mathbf{y}) \geq h(\mathcal{S}_\tau(\mathbf{z})) + \frac{1}{\tau}(\mathbf{z} - \mathcal{S}_\tau(\mathbf{z}))^\top (\mathbf{y} - \mathcal{S}_\tau(\mathbf{z})) - \tau 4nd^2.$$

By Definition 2 this establishes

$$\mathbf{z} - \mathcal{S}_\tau(\mathbf{z}) \in \tau \partial_{\tau \epsilon_2} h(\mathcal{S}_\tau(\mathbf{z})),$$

where $\epsilon_2 = 4nd^2$. This establishes the desired result for Part (c). \square

Corollary 1. For any $\tau > 0$ and for any $\mathbf{z} \in \mathbb{R}^n$

$$\|\text{prox}_{\tau h}(\mathbf{z}) - \mathcal{S}_\tau(\mathbf{z})\|_2 \leq \tau \epsilon_1 .$$

Proof. Define function Φ_τ for $\mathbf{z} \in \mathbb{R}^n$ as

$$\Phi_\tau(\mathbf{x}) = \frac{1}{2\tau} \|\mathbf{x} - \mathbf{z}\|_2^2 + \tau h(\mathbf{x}) .$$

By using Proposition 2.5 (2.) of [48] with this paper's Proposition 2 (b), we have

$$\begin{aligned} \mathcal{S}_\tau(\mathbf{z}) &= \text{prox}_{\tau h}(\mathbf{z} + \boldsymbol{\delta}) \quad \text{where} \quad \|\boldsymbol{\delta}\|_2 \leq \tau \epsilon_1 \\ &\implies \\ 0 &\in \partial_{(\tau \epsilon_1)^2 / (2\tau)} \Phi_\tau(\mathcal{S}_\tau(\mathbf{z})) . \end{aligned}$$

Using [43, 44] implies that

$$\|\text{prox}_{\tau h}(\mathbf{z}) - \mathcal{S}_\tau(\mathbf{z})\|_2 \leq \tau \epsilon_1 .$$

□

Lemma 1. For both the anisotropic and isotropic versions, any subgradient $\mathbf{g} \in \partial \bar{h}(\mathbf{u})$ has a bounded l_2 norm $\|\mathbf{g}\|_2 \leq 2d\sqrt{n}$.

Proof. This lemma makes use of the following subdifferential sum property: for any f_1, \dots, f_m real valued convex functions

$$\partial \left[\sum_{i=1}^m f_i \right] (\mathbf{x}) = \sum_{i=1}^m \partial f_i(\mathbf{x}) \quad \forall \mathbf{x} \in \mathbb{R}^n . \quad (25)$$

First consider the anisotropic version

$$\bar{h}^a(\mathbf{u}) = 2\sqrt{d} \|\mathbf{u}^{\text{dif}}\|_{1,1} = 2\sqrt{d} \sum_{i=1}^n \|[\mathbf{u}^{\text{dif}}]_i\|_1 .$$

Consider $\partial(\|[\mathbf{u}^{\text{dif}}]_i\|_1)$, whose norm is bounded by \sqrt{d} . By Eq. (25), letting $\mathbf{g} \in \partial \bar{h}^a(\mathbf{u})$, we can bound

$$\begin{aligned} \|\mathbf{g}\|_2 &= 2\sqrt{d} \sqrt{\sum_{i=1}^n \left(\partial(\|[\mathbf{u}^{\text{dif}}]_i\|_1) \right)^2} \\ &\leq (2\sqrt{d}) \sqrt{n(\sqrt{d})^2} \\ &= 2d\sqrt{n} . \end{aligned}$$

Now consider the isotropic version

$$\bar{h}^i(\mathbf{u}) = 2\sqrt{d} \|\mathbf{u}^{\text{dif}}\|_{2,1} = 2\sqrt{d} \sum_{i=1}^n \|[\mathbf{u}^{\text{dif}}]_i\|_2 .$$

Consider $\partial(\|[\mathbf{u}^{\text{dif}}]_i\|_2)$, whose norm is bounded by 1. By Eq. (25), letting $\mathbf{g} \in \partial \bar{h}^i(\mathbf{u})$, we obtain the bound

$$\|\mathbf{g}\|_2 = 2\sqrt{d} \sqrt{\sum_{i=1}^n \left\| \partial(\|[\mathbf{u}^{\text{dif}}]_i\|_2) \right\|_2^2} \leq 2\sqrt{nd} .$$

Since $d \geq 1$, we have $2\sqrt{nd} \leq 2d\sqrt{n}$. Therefore, for both the anisotropic and isotropic, $\|\mathbf{g}\|_2$ is bounded by $2d\sqrt{n}$. □

References

- [1] L. I. Rudin, S. Osher, and E. Fatemi, “Nonlinear total variation based noise removal algorithms,” *Physica D*, vol. 60, no. 1–4, pp. 259–268, Nov. 1992.
- [2] Neal Parikh and Stephen Boyd, “Proximal algorithms,” *Foundations and Trends in Optimization*, vol. 1, no. 3, pp. 127–239, 2014.
- [3] A. Beck and M. Teboulle, “A fast iterative shrinkage-thresholding algorithm for linear inverse problems,” *SIAM J. Imag. Sciences*, vol. 2, no. 1, pp. 183–202, 2009.
- [4] S. Boyd, N. Parikh, E. Chu, B. Peleato, and J. Eckstein, “Distributed optimization and statistical learning via the alternating direction method of multipliers,” *Found. and Trends in Mach. Learn.*, vol. 3, no. 1, pp. 1–122, Jul. 2011.
- [5] A. Beck and M. Teboulle, “Fast gradient-based algorithm for constrained total variation image denoising and deblurring problems,” *IEEE Trans. Image Process.*, vol. 18, no. 11, pp. 2419–2434, Nov. 2009.
- [6] Tom Goldstein and Stanley Osher, “The split Bregman method for l_1 -regularized problems,” *SIAM Journal on Imaging Sciences*, vol. 2, no. 2, pp. 323–343, 2009.
- [7] U. S. Kamilov, E. Bostan, and M. Unser, “Variational justification of cycle spinning for wavelet-based solutions of inverse problems,” *IEEE Signal Process. Lett.*, vol. 21, no. 11, pp. 1326–1330, Nov. 2014.
- [8] U. S. Kamilov, “Parallel proximal methods for total variation minimization,” in *IEEE Int. Conf. Acoust., Speech Signal Process.*, Shanghai, China, Mar. 19–25, 2016, pp. 4697–4701.
- [9] U. S. Kamilov, “A parallel proximal algorithm for anisotropic total variation minimization,” *IEEE Trans. Image Process.*, vol. 26, no. 2, pp. 539–548, Feb. 2017.
- [10] U. S. Kamilov, “Minimizing isotropic total variation without subiterations,” in *Proc. 3rd Int. Travel. Workshop Interac. between Sparse models and Tech.*, Aalborg, Denmark, Aug. 24–26, 2016.
- [11] Y.-L. Yu, “Better approximation and faster algorithm using the proximal average,” in *Proc. Advances in Neural Information Processing Systems 26*, Lake Tahoe, CA, USA, December 5–10, 2013, pp. 458–466.
- [12] M. M. Bronstein, A. M. Bronstein, M. Zibulevsky, and H. Azhari, “Reconstruction in diffraction ultrasound tomography using nonuniform FFT,” *IEEE Trans. Med. Imag.*, vol. 21, no. 11, pp. 1395–1401, Nov. 2002.
- [13] M. V. Afonso, J. M. Bioucas-Dias, and M. A. T. Figueiredo, “Fast image recovery using variable splitting and constrained optimization,” *IEEE Trans. Image Process.*, vol. 19, no. 9, pp. 2345–2356, Sep. 2010.
- [14] E. J. Candès, J. Romberg, and T. Tao, “Robust uncertainty principles: Exact signal reconstruction from highly incomplete frequency information,” *IEEE Trans. Inf. Theory*, vol. 52, no. 2, pp. 489–509, Feb. 2006.
- [15] M. Lustig, D. L. Donoho, and J. M. Pauly, “Sparse MRI: The application of compressed sensing for rapid MR imaging,” *Magn. Reson. Med.*, vol. 58, no. 6, pp. 1182–1195, Dec. 2007.
- [16] C. Louchet and L. Moisan, “Total variation denoising using posterior expectation,” in *Eur. Signal Process. Conf.*, Lausanne, Switzerland, Aug. 25–29, 2008.
- [17] J. P. Oliveira, J. M. Bioucas-Dias, and M. A. T. Figueiredo, “Adaptive total variation image deblurring: A majorization-minimization approach,” *Signal Process.*, vol. 89, no. 9, pp. 1683–1693, Sep. 2009.
- [18] U. S. Kamilov, I. N. Papadopoulos, M. H. Shoreh, A. Goy, C. Vonesch, M. Unser, and D. Psaltis, “A learning approach to optical tomography,” in *Front. in Opt. 2015*. 2015, p. LW3I.1, Optical Society of America.
- [19] Zhaoyan Qu, Ximing Yan, Jinxiao Pan, and Ping Chen, “Sparse view CT image reconstruction based on total variation and wavelet frame regularization,” *IEEE Access*, vol. 8, pp. 57400–57413, 2020.
- [20] J. Liu, Y. Sun, X. Xu, and U. S. Kamilov, “Image restoration using total variation regularized deep image prior,” in *IEEE Int. Conf. Acoust., Speech Signal Process.*, May 2019, pp. 7715–7719.
- [21] Juncheng Guo and Qinghua Chen, “Image denoising based on nonconvex anisotropic total-variation regularization,” *Signal Process.*, vol. 186, pp. 108124, 2021.
- [22] Xiangyang Kong, Yongqiang Zhao, Jonathan Cheung-Wai Chan, and Jize Xue, “Hyperspectral image restoration via spatial-spectral residual total variation regularized low-rank tensor decomposition,” *Remote Sens.*, vol. 14, no. 3, pp. 511, Jan. 2022.

- [23] Yong Chen, Wei He, Naoto Yokoya, and Ting-Zhu Huang, “Hyperspectral image restoration using weighted group sparsity-regularized low-rank tensor decomposition,” *IEEE Trans. Cybernet.*, vol. 50, no. 8, pp. 3556–3570, Aug. 2020.
- [24] Saori Takeyama, Shunsuke Ono, and Itsuo Kumazawa, “Hyperspectral image restoration by hybrid spatio-spectral total variation,” in *IEEE Int. Conf. Acoust., Speech Signal Process.*, Mar. 2017, pp. 4586–4590.
- [25] Ge Ma, Ziwei Yan, Zhifu Li, and Zhijia Zhao, “Efficient iterative regularization method for total variation-based image restoration,” *Electronics*, vol. 11, no. 2, pp. 258, Jan. 2022.
- [26] Manoj Diwakar, Prabhishkek Singh, and Deepak Garg, “Edge-guided filtering based CT image denoising using fractional order total variation,” *Biomed. Signal Process. and Control*, vol. 92, pp. 106072, Jun. 1, 2024.
- [27] Antonin Chambolle and Thomas Pock, “An introduction to continuous optimization for imaging,” *Acta Numerica*, vol. 25, pp. 161–319, May 2016.
- [28] Xiaoqiang Luo, Wei Yu, and Chengxiang Wang, “An image reconstruction method based on total variation and wavelet tight frame for limited-angle CT,” *IEEE Access*, vol. 6, pp. 1461–1470, 2018.
- [29] Ajinkya Kadu, Hassan Mansour, and Petros T. Boufounos, “High-Contrast Reflection Tomography With Total-Variation Constraints,” *IEEE Trans. Comput. Imag.*, vol. 6, pp. 1523–1536, 2020.
- [30] L. Condat, “A direct algorithm for 1-D total variation denoising,” *IEEE Signal Process. Lett.*, vol. 20, no. 11, pp. 1054–1057, Nov. 2013.
- [31] S. Mallat, *A Wavelet Tool of Signal Processing: The Sparse Way*, Academic Press, San Diego, 3rd edition, 2009.
- [32] R. R. Coifman and D. L. Donoho, *Springer Lecture Notes in Statistics*, chapter Translation-invariant de-noising, pp. 125–150, Springer-Verlag, 1995.
- [33] A. K. Fletcher, K. Ramchandran, and V. K. Goyal, “Wavelet denoising by recursive cycle spinning,” in *Proc. IEEE Int. Conf. Image Process. (ICIP’02)*, Rochester, NY, USA, Sep. 2002, pp. II.873–II.876.
- [34] M. A. T. Figueiredo and R. D. Nowak, “An EM algorithm for wavelet-based image restoration,” *IEEE Trans. Image Process.*, vol. 12, no. 8, pp. 906–916, Aug. 2003.
- [35] C. Vonesch and M. Unser, “A fast thresholded Landweber algorithm for wavelet-regularized multidimensional deconvolution,” *IEEE Trans. Image Process.*, vol. 17, no. 4, pp. 539–549, Apr. 2008.
- [36] C. Vonesch and M. Unser, “A fast multilevel algorithm for wavelet-regularized image restoration,” *IEEE Trans. Image Process.*, vol. 18, no. 3, pp. 509–523, Mar. 2009.
- [37] M. Guerquin-Kern, M. Häberlin, K. P. Prüssmann, and M. Unser, “A fast wavelet-based reconstruction method for magnetic resonance imaging,” *IEEE Trans. Med. Imag.*, vol. 30, no. 9, pp. 1649–1660, Sep. 2011.
- [38] S. Ramani and J. A. Fessler, “A hybrid regularizer combining orthonormal wavelets and finite differences for statistical reconstruction in 3-D CT,” in *Proc. 2nd Intl. Mtg. Image Form. in X-ray CT*, Salt Lake City, UT, USA, 2012, pp. 348–351.
- [39] U. S. Kamilov, E. Bostan, and M. Unser, “Wavelet shrinkage with consistent cycle spinning generalizes total variation denoising,” *IEEE Signal Process. Lett.*, vol. 19, no. 4, pp. 187–190, Apr. 2012.
- [40] Eric A. Borisch, Adam T. Froemming, Roger C. Grimm, Akira Kawashima, Joshua D. Trzasko, and Stephen J. Riederer, “Model-based image reconstruction with wavelet sparsity regularization for through-plane resolution restoration in t2-weighted spin-echo prostate MRI,” *Magn. Reson. Med.*, vol. 89, no. 1, pp. 454–468, Jan. 2023.
- [41] Frank Ong, Joseph Y. Cheng, and Michael Lustig, “General phase regularized reconstruction using phase cycling,” *Magn. Reson. Med.*, vol. 80, no. 1, pp. 112–125, 2018.
- [42] N. Teyfour, Hossein Rabbani, and I. Jabbari, “Low-dose cone-beam computed tomography reconstruction through a fast three-dimensional compressed sensing method based on the three-dimensional pseudo-polar Fourier transform,” *J. Med. Signals and Sensors*, vol. 12, no. 1, pp. 8–24, Dec. 28, 2021.
- [43] R. T. Rockafellar, “Monotone operators and the proximal point algorithm,” *SIAM J. Control and Optim. Sciences*, vol. 14, no. 5, pp. 877–898, 1976.
- [44] Osman Güler, “New proximal point algorithms for convex minimization,” *SIAM J. Optim.*, vol. 2, no. 4, pp. 649–664, Nov. 1992.
- [45] J.-F. Aujol and Ch. Dossal, “Stability of over-relaxations for the forward-backward algorithm, application to FISTA,” *SIAM J. Optim.*, vol. 25, no. 4, pp. 2408–2433, Jan. 2015.

- [46] A. d’Aspremont, “Smooth optimization with approximate gradient,” *SIAM J. Optim.*, vol. 19, no. 3, pp. 1171–1183, 2008.
- [47] O. Devolder, F. Glineur, and Y. Nesterov, “First-order methods of smooth convex optimization with inexact oracle,” *Math. Program. Ser. A*, vol. 146, no. 1-2, pp. 37–75, 2013.
- [48] Saverio Salzo and Silvia Villa, “Inexact and accelerated proximal point algorithms,” *J. Convex Analysis*, vol. 19, no. 4, pp. 1167–1192, 2012.
- [49] Silvia Villa, Saverio Salzo, Luca Baldassarre, and Alessandro Verri, “Accelerated and inexact forward-backward algorithms,” *SIAM J. Optim.*, vol. 23, no. 3, pp. 1607–1633, Jan. 2013.
- [50] M. Schmidt, N. Le Roux, and F. Bach, “Convergence rates of inexact proximal-gradient methods for convex optimization,” in *Proc. Adv. in Neural Inf. Proc. Syst.*, Granada, Spain, Dec. 12-15, 2011, vol. 24.
- [51] Yurii Nesterov, “Inexact accelerated high-order proximal-point methods,” *Math. Program Ser. B*, vol. 197, no. 1, pp. 1–26, Jan. 1, 2023.
- [52] Yunier Bello-Cruz, Max L. N. Gonçalves, and Nathan Krislock, “On inexact accelerated proximal gradient methods with relative error rules,” *arXiv:2005.03766*, May 7, 2020.
- [53] D. P. Bertsekas, “Incremental proximal methods for large scale convex optimization,” *Math. Program. Ser. B*, vol. 129, pp. 163–195, 2011.
- [54] M. Elad, P. Milanfar, and R. Rubinfeld, “Analysis versus synthesis in signal priors,” *Inverse Problems*, vol. 23, no. 3, pp. 947–968, 2007.
- [55] J. J. Moreau, “Proximité et dualité dans un espace hilbertien,” *Bulletin de la Société Mathématique de France*, vol. 93, pp. 273–299, 1965.
- [56] Ralph Tyrell Rockafellar, *Convex Analysis*, Princeton University Press, Princeton, 1970.
- [57] A. Brøndsted and R. T. Rockafellar, “On the subdifferentiability of convex functions,” *Proc. of the Amer. Math. Society*, vol. 16, no. 4, pp. 605–611, 1965.
- [58] D. J. Ching and D. Gürsoy, “XDesign: an open-source software package for designing X-ray imaging phantoms and experiments,” *J. Synchrotron Rad.*, vol. 24, no. 2, pp. 537–544, 2017.
- [59] Thilo Balke, Fernando Davis, Cristina Garcia-Cardona, Soumendu Majee, Michael McCann, Luke Pfister, and Brendt Wohlberg, “Scientific computational imaging code (SCICO),” *J. Open Source Software*, vol. 7, no. 78, pp. 4722, 2022.